Full Paper

Journal of the Brazilian Chemical Society

https://dx.doi.org/10.21577/0103-5053.20250113

J. Braz. Chem. Soc. **2025**, *36*, 11, e-20250113, 1-12

Platinum and other Metals Doped-Manganese Tungstate as a Novel Catalytic Support for $NaBH_4$ Hydrolysis and Hydrogen Evolution Under Mild Conditions

Jorge Luiz dos Santos,[a] Iterlandes Machado Junior,[a] Gabriel Henrique Sperandio,[a] Gessica do C. Dias,[a] Anderson Dias,[b] Geraldo M. de Lima[b] and Renata P. L. Moreira[a]*

[a]*Departamento de Química, Universidade Federal de Viçosa (UFV), Av. Peter Henry Rolfs, s/n, 36570-000 Viçosa-MG, Brazil*

[b]*Departamento de Química, Universidade Federal de Minas Gerais, Av. Presidente Antônio Carlos, 6627, 31270-901 Belo Horizonte-MG, Brazil*

Manganese tungstate ($MnWO_4$) was synthesized using the microwave-assisted hydrothermal method and decorated with platinum nanoparticles (Pt NPs). For the first time, this ceramic material was applied as a catalyst for hydrogen evolution through the hydrolysis of sodium borohydride ($NaBH_4$). The synthesis was confirmed through Fourier transform infrared spectroscopy (FTIR), X-ray diffraction (XRD), and Raman techniques, which revealed that the material crystallizes in a monoclinic structure of the wolframite-type. The presence of Pt NPs was verified by energy-dispersive X-ray spectroscopy (EDS), and their average size of 6.99 ± 0.48 nm was determined by high-resolution transmission electron microscopy (HRTEM), evidencing uniform distribution throughout the support. The material exhibited a hydrogen generation rate (HGR) of 4363 at 293.15 K and 5265 at 323.15 K, with an activation energy of 8.59 kJ mol^{-1} for a Pt NPs dosage of 0.025 mmol. Furthermore, the catalyst demonstrated satisfactory performance over 11 reuse cycles. This work presented the Pt NPs/$MnWO_4$ composite as an efficient and durable catalyst for H_2 production via $NaBH_4$ hydrolysis, highlighting its potential for applications in sustainable energy systems.

Keywords: $MnWO_4$, hydrogen storage, catalysis, metallic nanoparticles, sustainability, composites

Introduction

Currently, approximately 80% of global primary energy consumption comes from fossil fuels such as coal, oil, and natural gas. This excessive dependence on these polluting fuels is responsible for two-thirds of global greenhouse gas (GHG) emissions. Since the mid-18th century, the accumulation of GHGs in the atmosphere has increased at an alarming rate. This uncontrolled emission of gases, such as carbon dioxide (CO_2), is destabilizing the natural balance of Earth's radiation, causing unprecedented global warming.[1]

Amid growing environmental pollution and the energy crisis, molecular hydrogen (H_2) stands out as a clean and promising fuel.[2] This gas is an attractive alternative for a more sustainable future due to its relatively high calorific value (ca. 120 kJ g^{-1}), as well as its zero carbon emissions when used in energy generation.[2,3] Potential future applications of hydrogen energy span various fields, such as heating, transportation, mechanical power, and electricity generation.[4] However, due to its low density (0.0899 g L^{-1}) and boiling point (20.37 K), storage techniques such as gas compression or liquefaction remain economically unfeasible and pose safety concerns.[4,5]

Given this context, sodium borohydride ($NaBH_4$) has been extensively investigated as a promising candidate for solid-state hydrogen storage. This compound offers a high storage capacity of 10.8 wt.%, non-toxicity, and considerable stability both in solid form and in solution.[2,5] The hydrolysis reaction of sodium borohydride that releases hydrogen gas can be seen in equation 1:

$$NaBH_{4(aq)} + 4H_2O_{(l)} \rightarrow B(OH)_4^-{}_{(aq)} + 4\ H_{2(g)} \quad \Delta H = -210\ kJ \qquad (1)$$

*e-mail: renata.plopes@ufv.br
Editor handled this article: Juliano Alves Bonacin (Associate)

One gram of $NaBH_4$ generates 2.38 L of hydrogen under ambient conditions (25 °C and 1 atm).[6] However, despite the reaction being spontaneous and exothermic, its kinetics is considerably slow.[7] To increase the efficiency and speed of hydrogen production through the hydrolysis of $NaBH_4$, the use of catalysts plays a crucial role. Various works have demonstrated the presence of a wide range of materials capable of efficiently catalyzing the hydrolysis of $NaBH_4$, thereby accelerating the hydrogen generation rate (HGR). Among the catalysts, monometallic particles such as cobalt stand out,[2,4,8-17] copper,[18,19] niobium,[20] nickel,[21,22] palladium,[23] platinum,[24-27] rhodium,[28] ruthenium,[27,29-34] and bimetallic, such as nickel-cobalt,[5,35] nickel-platinum,[36,37] nickel-silver,[38] platinum-palladium,[39] and platinum-ruthenium.[40]

Catalysts in the form of nanoparticles demonstrate high catalytic activity due to their large surface area-to-volume ratio and quantum confinement effects. However, this high surface area also promotes self-aggregation, which tends to reduce their reactivity.[26] Directly depositing them onto support materials is a possible solution to enhance the stability of these nanoparticles, such as porous carbon structures,[41] zeolites,[42] mesoporous silicas,[43] porous organic polymers,[44] metal-organic frameworks (MOFs),[20,45] among other materials.

Among the ceramic compounds, Joaquín-Morales *et al.*[46] synthesized $MnWO_4$ using the coprecipitation method and applied it in hydrogen production through the water splitting process under visible light. According to the authors, hydrogen production rates were obtained in the range of 34-72 μmol H_2 g_{cat}^{-1}. Sethi *et al.*[47] synthesized $MnWO_4$ nanoparticles via a hydrothermal process, which were then decorated with CdS. The material was employed as a photocatalyst for hydrogen production from water photolysis under solar irradiation. The authors reported a hydrogen production rate of 3218 μmol h^{-1} g_{cat}^{-1}. Other works highlight manganese tungstate ($MnWO_4$) for its various applications, such as a photocatalyst,[48,49] high-performance supercapacitor,[50-52] potential component in light-emitting diodes (LEDs)[53] and a promising contrast agent in imaging techniques, including X-ray computed tomography and magnetic resonance imaging.[54]

The advancement of sustainable energy technologies depends on the development of highly efficient and stable catalysts for hydrogen production. Among the various materials used for solid-state hydrogen storage, hydrocarbons, hydrides, boron-based compounds, and imides/amides stand out.[55] Despite progress in this field, $MnWO_4$ has not yet been explored in the formulation of materials aimed at hydrogen release from solid-state storage. In this context, this study proposes the synthesis of $MnWO_4$ ceramics decorated with platinum nanoparticles (Pt NPs/$MnWO_4$) and investigates their potential for hydrogen evolution through the hydrolysis of sodium borohydride.

Experimental

Materials and reagents

All reagents used in this work were of analytical grade. Sodium borohydride 98% (CAS 16940-66-2), sodium hydroxide 95% (CAS 1310-73-2), and cobalt nitrate hexahydrate 98% (CAS 10026-22-9) were purchased from Vetec (Duque de Caxias/Rio de Janeiro, Brazil). Hexachloroplatinic acid(IV) hexahydrate (CAS No. 18497-13-7), nickel sulfate hexahydrate 98% (CAS 10101-97-0), and potassium tetrachloropalladate(II) 98% (CAS 10025-98-6) were purchased from Synth (Diadema/São Paulo, Brazil). Manganese(II) nitrate hydrate $Mn(NO_3)_2.xH_2O$ (CAS 15710-66-4) and sodium tungstate hydrate ($Na_2WO_4.2H_2O$) (CAS 10213-10-2) were both high-purity reagents (> 99%), purchased from Sigma-Aldrich (Duque de Caxias/Rio de Janeiro, Brazil).

All solutions were prepared using Type I water obtained from a Milli-Q system (Millipore Corporation, São Paulo/São Paulo, Brazil).

Synthesis of manganese tungstate

$MnWO_4$ was synthesized using the microwave-hydrothermal method according to the work of Siqueira and Dias.[56] Stoichiometric amounts of the precursor sodium tungstate dihydrate ($Na_2WO_4{\cdot}2H_2O$) and manganese(II) nitrate hydrate ($Mn(NO_3)_2.xH_2O$) were separately dissolved in deionized water and mixed under vigorous stirring. The resulting mixed solution (ca. 50 mL, pH = 8.9) was put in double-walled digestion vessels (100 mL of capacity) with an inner liner and cover made of Teflon tetrafluoromethoxyl (TFM) and an outer high-strength vessel shell made of polyetheretherketone (PEEK). A Milestone BatchSYNTH instrument (2.45 GHz) was used to conduct the synthesis under microwaves. The Easy Control software (version 5.4.1, Bosch, Italy, 2024) was employed to draw a temperature-pressure-time profile, which included a heating time of 2 min up to the processing temperature (150 °C), for 20 min, to produce the $MnWO_4$ (the final conditions were 150 ± 1 °C and 1.2 ± 0.2 bar). The magnetic stirring module ensured uniform agitation of solutions in all vessels, independent of their position within the cavity. After microwave syntheses, the products were rinsed with deionized water several times and dried at 70 °C. Calcination was also performed using microwave heating (Milestone) at 600 °C, in air, for 2 h.

Synthesis of monometallic and bimetallic nanoparticles decorated on $MnWO_4$

To obtain the catalyst, 50 mg of manganese tungstate were dispersed in 5 mL of Milli-Q water, and the system was stirred for 10 min. For the synthesis of monometallic nanoparticles, 5 mL of aqueous solutions containing metal precursors, such as $Co(NO_3)_2{\cdot}6H_2O$, $NiSO_4{\cdot}6H_2O$, K_2PdCl_4, and $H_2PtCl_6{\cdot}6H_2O$, equivalent to a total of 0.10 mmol of Co, Ni, Pd, and Pt, respectively, were separately added to the mixture. For the synthesis of bimetallic nanoparticles, 5 mL of each aqueous solution containing the precursors (metal 1 and metal 2) were added to the manganese tungstate, resulting in a total of 0.10 mmol of metal. The compositions were Co:Ni, Co:Pd, Co:Pt, Ni:Pd, Ni:Pt, and Pd:Pt, all in a 1:1 molar ratio. Finally, 1.00 mL of $NaBH_4$ solution (1.00 mol L^{-1}) was added to the system, and the mixture was stirred for 15 min at room temperature (ca. 20 °C). The resulting material was washed with Milli-Q water and centrifuged at 4000 rpm for 15 min, with the supernatant discarded after each centrifugation step. This process was repeated three times. The freshly prepared catalyst was immediately used for hydrogen evolution from $NaBH_4$.

Material characterization

The materials were characterized using different techniques. High-resolution transmission electron microscopy (HRTEM) was used to evaluate and determine the size of the metallic nanoparticles, employing a Tecnai G2-20 Supertwin FEI-200 kV microscope (Hillsboro, OR, USA).

Fourier transform infrared spectroscopy (FTIR) analyses were carried out using a spectrophotometer (ALPHA II, Bruker, USA) equipped with an attenuated total reflectance (ATR) accessory. Spectra were collected in the range of 400-4000 cm^{-1}, with 54 scans and a spectral resolution of 4 cm^{-1}.

Raman spectroscopy was performed using a MicroRaman InVia Renishaw instrument. A 633 nm wavelength laser with a power of 3 mW was used, with five accumulations and an integration time of 30 s *per* measurement.

The crystallinity of the material was evaluated by conventional X-ray diffraction (XRD) using a Bruker D8-Discovery diffractometer (Billerica, MA, USA) with copper as the target, employing Cu Kα radiation (λ = 1.5414 Å) in a Bragg-Brentano (θ-2θ) configuration. The scan speed was 0.05°2θ at 2.5 s^{-1} over a range of 5° to 40°.

The morphology of the reused materials was evaluated by scanning electron microscopy (SEM) using a JEOL JSM-6010LA electron microscope at an accelerating voltage of 20 kV. For the analysis, the samples were placed on carbon tape and coated with gold using a Quorum Q150R S coater.

Hydrogen evolution from $NaBH_4$

The freshly prepared catalyst was dispersed in 10.0 mL of Type I water inside a Kitassato flask sealed with a rubber septum. A hose was connected to the side outlet of the Kitassato and attached to a burette, following the methodology described by Junior *et al.*[5] The system was continuously stirred using a magnetic stirrer while maintaining temperature control. Subsequently, 1.00 mL of $NaBH_4$ solution (0.50 mol L^{-1}) was injected into the system using a syringe.

The volume (mL) of gas produced was measured by recording the displacement of water in the graduated column of the gas collector. The pressure (P) exerted by the hydrogen gas on the liquid column was calculated according to equation 2:

$$P = P_0 + \rho g h \quad (2)$$

where ρ is the water density (1000 kg m^{-3}), g is the gravitational acceleration (9.78 m s^{-2}), P_0 is the local atmospheric pressure (94258.65 Pa or 0.93 atm), and h is the observed displacement, given in meters.

The experiments were filmed, and the data were extracted for processing using the OriginPro 2021 software (OriginLab Corporation, United States, 2021).

Evaluation of reaction parameters

The evaluation of the reaction parameters involved varying different doses of the Pt NPs/$MnWO_4$ catalyst, different concentrations of NaOH, different concentrations of $NaBH_4$, different system temperatures, material reuse, and durability. The conditions for each process will be described in the following sections.

Influence of Pt NPs/$MnWO_4$ catalyst dose

Hydrogen evolution experiments were conducted using four different doses of the Pt NPs/$MnWO_4$ catalyst, with platinum quantities of 0.025, 0.050, 0.075, and 0.100 mmol, corresponding to metal contents of 8.88, 16.32, 22.64, and 28.06% (m/m), respectively. The other parameters, including 50 mg of support, 1.0 mL of $NaBH_4$ (0.50 mol L^{-1}), and temperature of 293.15 K, remained constant. The system remained under constant stirring.

Influence of NaOH concentration

The hydrogen evolution experiment was performed by dissolving $NaBH_4$ (0.50 mol L^{-1}) in NaOH solutions with concentrations of 0.010, 0.050, 0.100, and 0.200 mol L^{-1}. The other parameters, including a support mass of 50 mg, a Pt NPs/$MnWO_4$ dose of 0.025 mmol Pt (0.0049 g), and a temperature of 293.15 K, remained constant. The system remained under constant stirring.

Influence of $NaBH_4$ concentration

Hydrogen evolution experiments were conducted with four different concentrations of $NaBH_4$ (0.23, 0.33, 0.40, and 0.50 mol L^{-1}). The other parameters, including a support mass of 50 mg, a Pt NPs/$MnWO_4$ dose of 0.025 mmol Pt (0.0049 g), continuous stirring, and a temperature of 293.15 K, remained constant.

Influence of temperature

Hydrogen evolution experiments were carried out at different temperatures: 293.15; 303.15; 313.15; and 323.15 K. The other parameters, including a support mass of 50 mg, a Pt NPs/$MnWO_4$ dose of 0.025 mmol Pt (0.0049 g), continuous stirring, and 1.0 mL of $NaBH_4$ (0.50 mol L^{-1}), remained constant.

Catalyst reuse

The reuse of Pt NPs/$MnWO_4$ was evaluated. The initial conditions included a support mass of 50 mg, a Pt NPs/$MnWO_4$ dose of 0.025 mmol Pt (0.0049 g), 1.0 mL of $NaBH_4$ (0.50 mol L^{-1}), continuous stirring, and a temperature of 303.15 K. After each cycle, the resulting suspension was purified with 30 mL of Type I water, followed by centrifugation (4000 rpm, 15 min). The recovered solid was then dispersed in 10.0 mL of Type I water and reintroduced into the Kitassato for another cycle. This process was repeated until the 11th cycle.

Catalyst durability

The durability of Pt NPs/$MnWO_4$ was assessed. The initial conditions included a support mass of 50 mg, a Pt NPs/$MnWO_4$ dose of 0.025 mmol Pt (0.0049 g), 1.0 mL of $NaBH_4$ (0.50 mol L^{-1}), continuous stirring, and a temperature of 303.15 K. At the end of each cycle, a fresh $NaBH_4$ solution was introduced into the system without washing the catalyst. This process was repeated until the 11th cycle.

Determination of activation energy

Initially, the reaction kinetic constant was determined, according to equation 3, for each temperature used in the experiments: 293.15, 303.15, 313.15, and 323.15 K.

$$k = -\frac{4d\,[NaBH_4]}{dt} = \frac{d\,[H_2]}{dt} \quad (3)$$

The activation energy was calculated using the Arrhenius equation, equation 4:

$$\ln(k) = \ln(A) - \frac{Ea}{RT} \quad (4)$$

where k is the rate constant of the reaction, A is the pre-exponential factor, E_a is the apparent activation energy in kJ mol^{-1}, R is the universal gas constant, and T is the absolute temperature.

Hydrogen generation rate (HGR)

The hydrogen generation rate (HGR) was calculated according to equation 5:

$$HGR = \frac{\Delta V_{H_2}}{\Delta t \times m_{cat}} \quad (5)$$

where ΔV_{H_2} is the hydrogen volume variation (mL), Δt is the time variation (min), and m_{cat} is the catalyst mass (g).

During the development of this proposal, ChatGPT was used exclusively for grammatical review. All ideas and technical content are the sole responsibility of the authors.

Results and Discussion

Material characterization

FTIR analyses were performed for both $MnWO_4$ and Pt NPs/$MnWO_4$ nanoparticles, and the results are shown in Figure 1. The spectra are very similar, indicating that the incorporation of Pt NPs did not significantly alter the functional groups present in the material. A characteristic absorption band of $MnWO_4$ was observed in the region of 808 cm^{-1}, which can be attributed to the symmetric vibrations of Mn–W–O groups and the asymmetric stretching vibration of the short W–O bond.

Bands were also observed at 670 and 564 cm^{-1}, which can be attributed to the asymmetric stretching vibrations of the WO bond.[57] Similar results were obtained by other studies that synthesized $MnWO_4$ through different processes. Saranya *et al.*[58] synthesized a polyaniline (PANI)/$MnWO_4$ nanocomposite through *in situ* polymerization under ultrasonication. $MnWO_4$ was prepared using the surfactant-assisted ultrasonication method. The authors observed

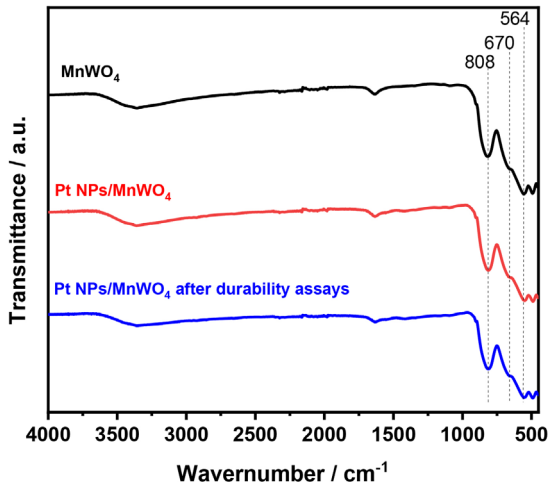

Figure 1. FTIR-ATR spectra of $MnWO_4$, Pt NPs/$MnWO_4$, and Pt NPs/$MnWO_4$ after durability assays.

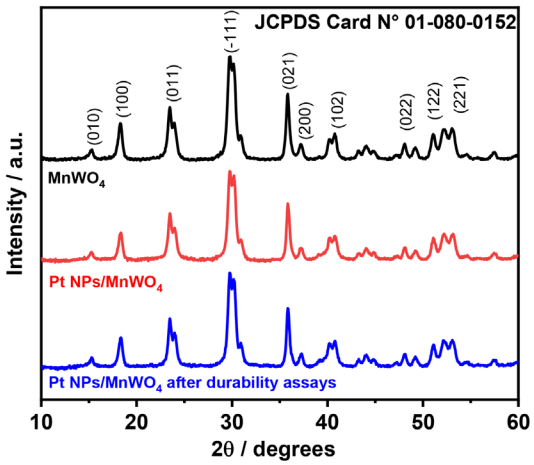

Figure 2. X-ray diffraction (XRD) patterns of $MnWO_4$, Pt NPs/$MnWO_4$, and Pt NPs/$MnWO_4$ after durability assays.

bands at 873, 805, 719, 598, and 445 cm^{-1}. Hoang *et al.*[49] synthesized $MnWO_4$ nanoparticles encapsulated in mesoporous silica ($MnWO_4$/SBA-15) using a microwave-assisted method. The authors observed characteristic bands at 880, 810, 700, and 590 cm^{-1}.

$MnWO_4$ and Pt nanoparticles supported on $MnWO_4$ were characterized by X-ray diffraction, and the results are shown in Figure 2. The diffractograms of both materials exhibited sharp and intense peaks at various 2θ values, reflecting a polycrystalline structure formed by multiple diffraction planes. XRD patterns were indexed to the monoclinic, wolframite-type structure, in agreement with the JCPDS Card No 01-080-0152. The presence of manganese tungstate in the composition of the materials was confirmed by the peaks at 2θ values of 15.3°, 18.3°, 23.5°, 24.0°, 29.8°, 30.2°, 30.9°, 35.9°, 37.2°, 40.3°, 40.8°, 48.2°, 49.2°, 51.1°, 52.4°, and 52.9°, which correspond to the Miller indices (010), (100), (011), (110), (–111), (111), (020), (021), (200), (–102), (102), (022), (200), (122), (202), and (221), respectively.[59] Furthermore, the absence of diffraction peaks associated with secondary phases indicates that the synthesized materials exhibit a high degree of purity. The similarity of the diffractograms demonstrates that the presence of Pt NPs in $MnWO_4$ did not significantly affect the positions of the crystallographic planes. Rathi *et al.*[60] synthesized $MnWO_4$ using $MnSO_4{\cdot}H_2O$ and $Na_2WO_4{\cdot}2H_2O$ precursors through a hydrothermal method at 120 °C for 24 h, yielding results comparable to those presented in this study. Kumar *et al.*[61] also synthesized $MnWO_4$ using $Na_2WO_4{\cdot}2H_2O$ and $Mn(CH_3COO)_2$ precursors via hydrothermal method at 180 °C for 12 h. According to the authors, the results obtained were similar to those of this work.

The results from Raman spectroscopy, shown in Figure 3, presented bands at 129, 164, 206, 257, 325, 396, 511, 543, 673, 697, 772, and 884 cm^{-1}, characteristic of $MnWO_4$, which crystallizes in a monoclinic arrangement of the wolframite-type, belonging to the *P2/c* space group with two units *per* unit cell.[62] The bands at 129, 164, and 206 cm^{-1} correspond to the translation modes of tungsten and manganese, while the band at 257 cm^{-1} corresponds to the twisting mode of the WO_2 group.[63] The peak at 326 cm^{-1} is attributed to the bending mode of the W–O–W group.[64] The bands at 396, 511, and 673 cm^{-1} are associated with the symmetric stretching vibration mode of W–O–W, while the peak at 543 cm^{-1} corresponds to the symmetric bending mode of W–O–W.[63] The symmetric stretching vibrational mode of the W–O bond corresponds to the band at 884 cm^{-1}, while the asymmetric stretching modes correspond to the bands at 697 and 772 cm^{-1}.[65] Both Pt NPs/$MnWO_4$ and $MnWO_4$ materials exhibited similar spectra due to the small dose of Pt NPs. These results are comparable to those obtained by Muthamizh *et al.*,[59] who synthesized $MnWO_4$ through surfactant-free precipitation. According to the authors, these materials were applied to modify the glassy carbon electrode (GCE) for quercetin detection. Furthermore, Shivaganga *et al.*[66] reported similar results when synthesizing $MnWO_4$ from $MnCl_2$ and $Na_2WO_4{\cdot}2H_2O$ using water as the sole solvent, through a method the authors defined as a green route. The compound was employed in the photodegradation of organic contaminants in water.

Figure S1 (Supplementary Information (SI) section) shows the results of the energy dispersive X-ray spectroscopy (EDS) analysis. It can be observed that, in the analyzed section, the catalyst is composed of tungsten (26.9%), oxygen (13.7%), manganese (7.1%), and platinum (46.3%). Additionally, the presence of sodium (1.8%) was identified, which may have originated from the reagents used in the synthesis. The presence of copper is due to the sample

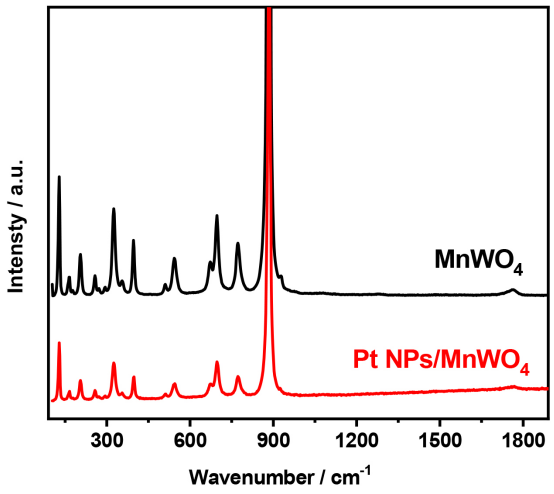

Figure 3. Raman spectra of $MnWO_4$, and Pt NPs/$MnWO_4$ materials.

holder used in the analysis. It is important to emphasize that EDS is a qualitative technique, and the elemental composition can vary significantly depending on the specific region analyzed. Therefore, the platinum content observed in this particular area may not represent the overall composition of the material. This reinforces the qualitative nature of the technique and helps explain the apparent discrepancy with the XRD results, where no characteristic diffraction peaks of platinum were observed. The absence of such peaks is likely due to the low overall concentration and high dispersion of the Pt nanoparticles, making them undetectable by XRD.

HRTEM analyses confirmed the successful deposition of platinum nanoparticles (Pt NPs) on the support, as shown in Figure 4. A leaf-like structure can be observed, attributed to manganese tungstate. The interplanar distance was calculated to be 0.238 nm, and the diffraction planes were indexed to the (200) crystalline plane of monoclinic $MnWO_4$, as shown in Figures 4a-4c.[66]

The results obtained are similar to those found by Lei *et al.*,[67] who synthesized $MnWO_4$ using the surfactant-assisted complexation-precipitation method at low temperature (150 °C). The authors found an interplanar distance of 0.242 nm, attributed to the (200) plane of monoclinic $MnWO_4$. Assis *et al.*[68] synthesized $MnWO_4$ via microwave-assisted hydrothermal method.

Pt NPs nanoparticles reached an average size of 6.99 ± 0.48 nm, as shown in the histogram of Figure 4d. They exhibited spherical morphology, were well dispersed on the smooth and uniform surface of the support, and showed an interplanar distance of 0.160 nm, as shown in Figures 4d-4f. Trombetta *et al.*[69] reported similar results during the synthesis of catalysts via direct reduction with sodium borohydride on a carbon support. The catalytic performances of both the synthesized PtMo/C and the commercial Pt/C catalysts were evaluated in a proton exchange membrane fuel cell (PEMFC).

Hydrogen evolution

The catalytic performance of Pt NPs/$MnWO_4$ was evaluated for hydrogen generation efficiency from $NaBH_4$

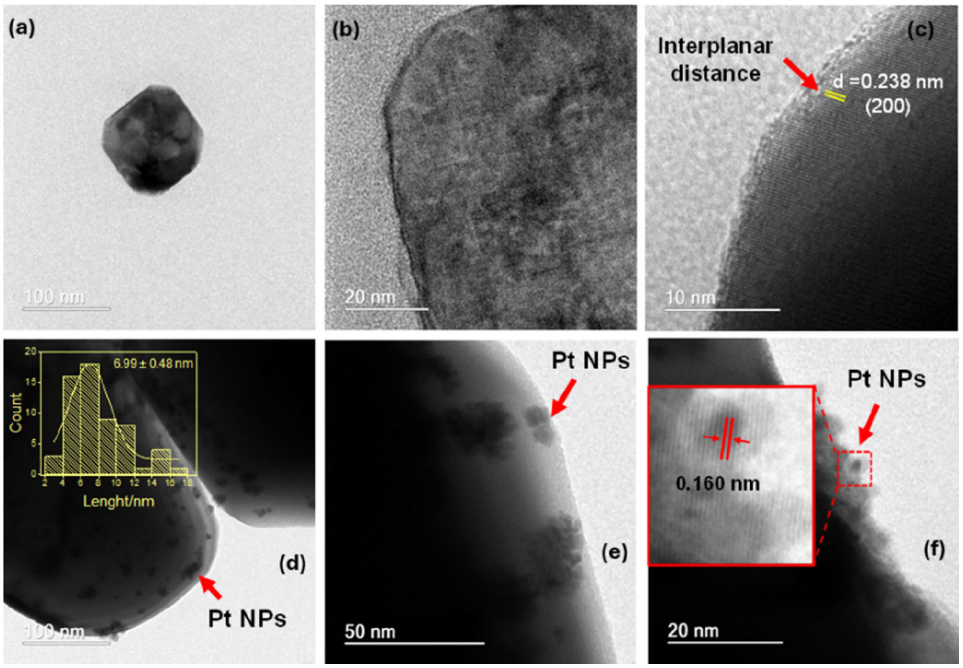

Figure 4. High-resolution transmission electron microscopy (HRTEM) images of (a-c) manganese tungstate ($MnWO_4$), and (d-f) support decorated with platinum nanoparticles Pt NPs/$MnWO_4$.

under different conditions, and the results are shown in Figure 5.

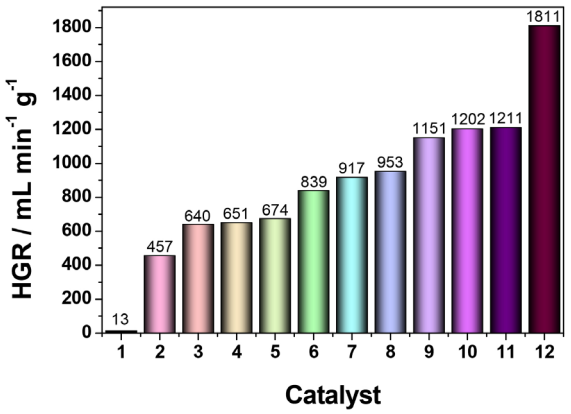

Figure 5. Hydrogen evolution from $NaBH_4$ mediated by nanoparticles decorated on $MnWO_4$. Experimental conditions: 1.00 mL of $NaBH_4$ (0.500 mol L^{-1}), $MnWO_4$: 50 mg, 0.10 mmol of metal, and temperature of 293.15 K. (1) $MnWO_4$, (2) Pd NPs/$MnWO_4$, (3) unsupported Pt NPs, (4) Co/Ni (1:1) NPs/$MnWO_4$, (5) Ni/Pd (1:1) NPs/$MnWO_4$, (6) Ni NPs/$MnWO_4$, (7) Co/Pt (1:1) NPs/$MnWO_4$, (8) Ni/Pt (1:1) NPs/$MnWO_4$, (9) Co NPs/$MnWO_4$, (10) Co/Pd (1:1) NPs/$MnWO_4$, (11) Pd/Pt (1:1) NPs/$MnWO_4$, and (12) Pt NPs/$MnWO_4$.

Among the monometallic nanoparticles, Pt NPs/$MnWO_4$ exhibited a HGR of 1811 mL min^{-1} g_{cast}^{-1} and a yield of 74%. It can be observed that the support alone presented a low HGR of 13 mL min^{-1} g_{cast}^{-1}, while Pt NPs without the support showed an HGR of 640 mL min^{-1} g_{cast}^{-1} and a yield of 66%. These results suggest a synergistic effect between the metal (Pt NPs) and the support ($MnWO_4$), leading to higher efficiency and faster kinetics. Among the bimetallic compositions, Pd-Pt NPs/$MnWO_4$ (1:1) exhibited the best performance with an HGR of 1211 mL min^{-1} g_{cast}^{-1}. However, both the yield and the HGR were lower than those of Pt NPs/$MnWO_4$, suggesting non-synergistic effect between Pt and Pd NPs.

Pt NPs/$MnWO_4$ exhibited a higher HGR than several values reported in the literature. Biehler *et al.*[70] synthesized carbon spheres derived from sugar decorated with platinum nanoparticles (PtFCS) and achieved an HGR of 18 mL min^{-1} g_{cast}^{-1} at 22 °C. Altaf *et al.*[71] used titanium dioxide as a platinum support (Pt/TiO_2) and obtained an HGR of 71 mL min^{-1} g_{cast}^{-1}. Kojima *et al.*[72] used a material consisting of Pt decorated on metal oxide (Pt-$LiCoO_2$), achieving an HGR of 3100 mL min^{-1} g_{cast}^{-1}. Based on these values, it can be concluded that Pt NPs/$MnWO_4$ is a highly promising material. Therefore, different parameters were evaluated in the hydrogen evolution catalysis from $NaBH_4$.

Evaluation of the $NaBH_4$ concentration effect

The effect of $NaBH_4$ concentration on the H_2 generation rate was evaluated, and the results are shown in Figure 6. It can be observed that the volume (mL) remains nearly unchanged for up to about 25 s, regardless of the $NaBH_4$ concentration. Figure S2 (SI section) shows the graph of the natural logarithm of the kinetic constant *versus* the natural logarithm of the $NaBH_4$ concentration, with an almost horizontal line and a slope of 0.0297. The slope of the linear model indicates that the catalysis by Pt NPs/$MnWO_4$ follows a zero-order reaction concerning the $NaBH_4$ concentration.

The rate law for the catalytic hydrolysis of $NaBH_4$ mediated by Pt NPs/$MnWO_4$ as a function of the $NaBH_4$ concentration is provided in equation 6.

$$r \propto [BH_4^-]^{0.0297} \quad (6)$$

The observation of a zero-order reaction with respect to $NaBH_4$ concentration has been previously reported in the literature. Junior *et al.*[5] and Sperandio *et al.*[37] reported similar results in their studies with metallic nanoparticle catalysts.

Evaluation of the platinum nanoparticle dose effect

The effect of platinum nanoparticle dose on hydrogen evolution using Pt NPs/$MnWO_4$ was evaluated, and the results are presented in Figure 6b. It was observed that increasing the Pt NPs dose from 0.025 to 0.100 mmol did not significantly affect the yield, which remained close to 70%. The HGR was measured at 293.15 K, yielding values of 4363 and 1811 mL min^{-1} g_{cast}^{-1} at Pt NP doses of 0.0250 mmol and 0.1000 mmol, respectively. Akbayrak *et al.*[73] utilized cobalt ferrite ($CoFe_2O_4$) decorated with Pt NPs for hydrogen evolution from ammonia borane. According to the authors, the reduction in catalytic activity with increasing platinum loading may be attributed to nanoparticle agglomeration.

Figure S3 (SI section) shows the plot of the natural logarithm of the rate constant (ln k) as a function of the natural logarithm of the Pt NPs dose (ln [Pt NPs]), with a slope of 0.4236. This observation suggests that the reaction exhibits pseudo-zero-order behavior concerning the catalyst amount used. The rate law for the catalytic hydrolysis of $NaBH_4$ mediated by Pt NPs/$MnWO_4$ as a function of the Pt NP dose is provided in equation 7.

$$r \propto [\text{Pt NPs}]^{0.4236} \quad (7)$$

Effect of NaOH concentration

Sodium hydroxide is known to enhance the efficiency

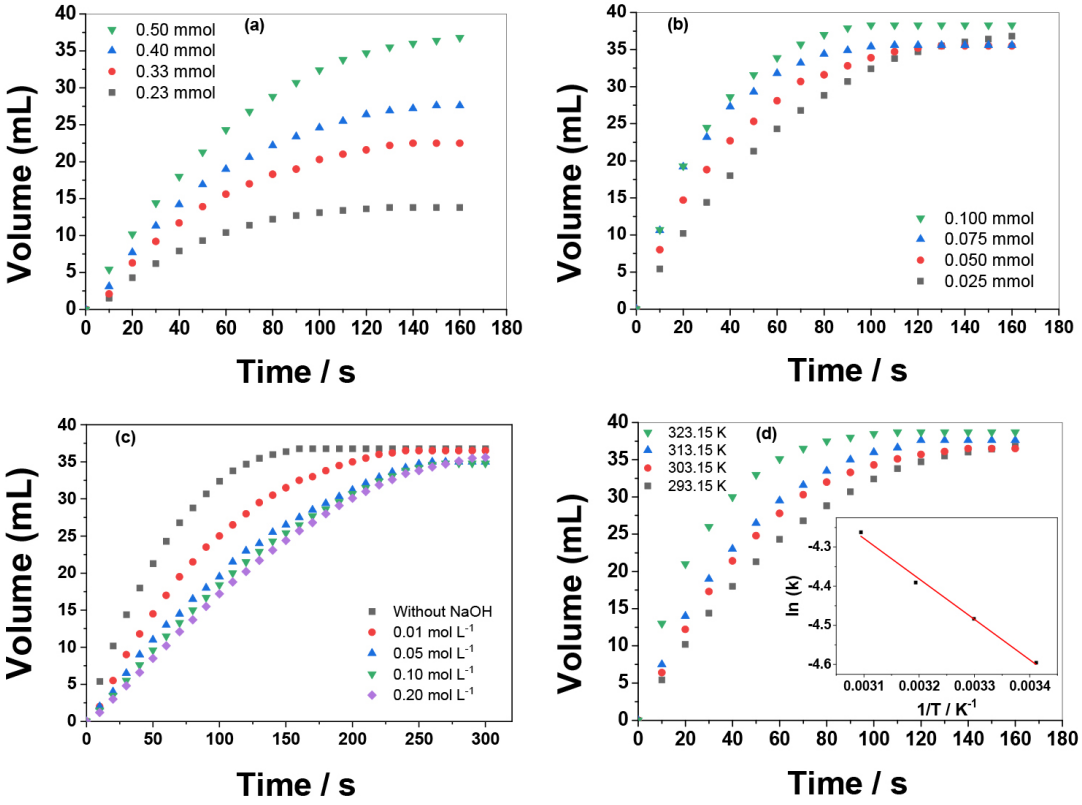

Figure 6. Hydrogen evolution mediated by Pt NPs/$MnWO_4$. (a) Evaluation of the $NaBH_4$ concentration effect. (b) Evaluation of the Pt NPs dose effect. (c) Evaluation of different NaOH concentrations. (d) Evaluation of the temperature.

of metal nanoparticle-based catalysts in the hydrolysis of $NaBH_4$. This improvement is attributed to the coordination of OH^- ions to the nanoparticle surface, leading to an increase in electronic density.[26] Thus, the oxidative addition of O–H, a typical step in the sodium borohydride hydrolysis mediated by metal, is enhanced.[74] Therefore, the effect of NaOH concentration was evaluated, and the results are shown in Figure 6c. It can be observed that the addition of NaOH decreased the efficiency of the process. The HGR of 4363 mL min^{-1} g_{cast}^{-1}, obtained under the condition without NaOH, decreased to 3300, 2504, 2328, and 2156 mL min^{-1} g_{cast}^{-1} with NaOH concentrations of 0.01, 0.05, 0.10, and 0.20 mol L^{-1}, respectively. Figure S4 (SI section) presents the graph of the natural logarithm of the kinetic constant *vs*. the natural logarithm of the NaOH concentration, highlighting an almost horizontal line with a slope of –0.1070. Based on these results, it can be concluded that the presence of the base decreases the hydrogen generation efficiency. Similar results have been reported by other authors.[70,75] According to dos Reis *et al*.,[36] such results may be related to the high electron density on the surface of Pt NPs, where OH^- ions compete with BH_4^- molecules for active sites, thus reducing the catalytic activity.

The rate law was proposed after evaluating the $NaBH_4$ concentration, Pt NPs dose, and NaOH concentration, as shown in equation 8.

$$r = k * [BH_4^-]^{0.0297} * [catalyst]^{0.4236} * [NaOH]^{-0.1070} \quad (8)$$

Effect of temperature

The effect of temperature on the $NaBH_4$ hydrolysis reaction mediated by Pt NPs/$MnWO_4$ nanoparticles was evaluated, as shown in Figure 6d. The data indicate that increasing the temperature results in higher reaction rates. From the kinetic constants, an Arrhenius plot was constructed (insert Figure 6d), whose linear fit to the experimental data showed a coefficient of determination of 0.991. The system revealed an activation energy of only 8.59 kJ mol^{-1}, with HGR of 4363 mL min^{-1} g_{cast}^{-1} at 293.15 K and 5265 mL min^{-1} g_{cast}^{-1} at 323.15 K, using 0.025 mmol of Pt nanoparticles (Figure S5, SI section).

These results indicate that the Pt NPs/$MnWO_4$ catalyst offers advantages over other platinum-containing catalytic systems, particularly regarding activation energy, as shown in Table 1. The obtained value is lower than those reported for systems such as Pt/C (36 kJ mol^{-1}),[24] Pt/MWCNT (multi-walled carbon nanotube) (27 kJ mol^{-1}),[24] and PtNP@PPh_2-PEGPILLS (polyethylene glycol modified

imidazolium monomer immobilized ionic liquids) (23.9 kJ mol^{-1}).[26] A comparative analysis also shows that the developed catalyst performs better than materials like Pt/TiO_2 (53.2 kJ mol^{-1}),[71] and PtFCS (53 kJ mol^{-1}),[70] whose activation energies are roughly six times higher. Although the HGR of Pt NPs/$MnWO_4$ (4363 mL min^{-1} g_{cast}^{-1} at 293.15 K) is comparable to that of commercial Pt/C (4569.6 mL min^{-1} g_{cast}^{-1}),[24] its lower activation energy may offer an important benefit. The catalyst exhibits a favorable thermal response, demonstrated by a 20% increase in HGR between 293.15 and 323.15 K, alongside a low activation energy, indicating strong potential for practical applications. Compared to more complex systems such as PtNP@PPh2-PEGPIILS, Pt NPs/$MnWO_4$ distinguishes itself not only through its performance but also due to its simpler synthesis and greater scalability.

Table 1. Different Pt-based catalysts used for hydrogen evolution from $NaBH_4$

Material	HGR / (mL min^{-1} g_{cat}^{-1})	E_a / (kJ mol^{-1})	Reference
Pt/MWCNT	1008[a]	27	24
Pt/C	4569.6[a]	36	24
PtNP@PPh_2-PEGPIILS	3786[b]	23.9	26
PtFCS	43.8[a]	53	70
PtNPs	0.816[c]	39.2	75
Pt/TiO_2	100	53.2	71
Pt NPs/$MnWO_4$	4363	8.59	this work

[a]Calculated based on the principle that 1 mol of an ideal gas occupies 22.4 L under standard temperature and pressure conditions; [b]L min^{-1} mol_{cat}^{-1} ; [c] mL min^{-1} mL_{cat}^{-1}. HGR: hydrogen generation rate; E_a: activation energy; Pt NPs: platinum nanoparticles; PEGPIILS: polyethylene glycol modified imidazolium monomer immobilized ionic liquids; MWCNT: multi-walled carbon nanotube; PtFCS: platinum nanoparticles supported on a fused carbon sphere composite.

Reuse and durability

Catalysts with regenerative capacity and potential for reuse and durability are essential for the economic and environmental viability of many industrial processes. The evaluation of these parameters for the Pt NPs/$MnWO_4$ material is shown in Figure 7. Regarding reuse assays, the material demonstrated good catalytic performance with a loss of efficiency (< 22%) observed only after the 11th cycle. The decrease in reuse capacity and durability of the material can be attributed to the blockage and inactivation of active sites caused by the precipitation of $NaBO_2$ on the catalyst surface during the hydrolysis reaction of $NaBH_4$.[76,77]

As for durability, the catalytic efficiency of the material was evaluated over successive cycles in hydrogen evolution assays from $NaBH_4$ without intermediate washing steps. The most significant drop in efficiency, around 35%, was identified after the 11th cycle, indicating the potential of the material for reuse in multiple catalytic cycles. Figure 1 and particularly Figure 2 (XRD) were performed to assess the cause of the observed decrease in durability, indicating that the structure of the material remained intact after the durability cycles. While EDS analysis (Figure S6, SI section) suggested a reduction in the Pt NPs content, potentially influencing the catalytic activity, the material continued to show promising performance even after 10 cycles of use.

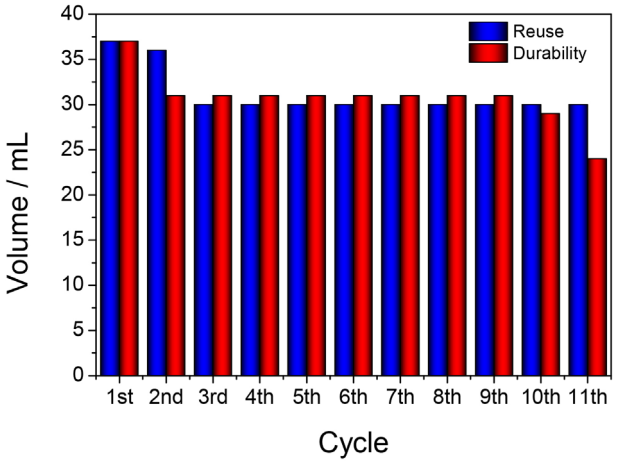

Figure 7. Evaluation of reuse and durability of the Pt NPs/$MnWO_4$ catalyst over different cycles. Experimental conditions: 1.00 mL of $NaBH_4$ (0.500 mol L^{-1}), $MnWO_4$: 50 mg, 0.025 mmol of metal, and temperature of 303.15 K.

Conclusions

This work investigated the effectiveness of manganese tungstate ($MnWO_4$) decorated with platinum nanoparticles (Pt NPs) as a catalyst for the hydrolysis reaction of sodium borohydride ($NaBH_4$) aimed at hydrogen production. Characterization techniques such as FTIR, XRD, Raman, EDS, and HRTEM confirmed the successful synthesis of the material and the uniform deposition of platinum nanoparticles on the support. The combination of the noble metal and the support exhibited a satisfactory synergistic effect, enhancing hydrogen evolution efficiency. The catalytic assays demonstrated that the synthesized material performs comparably to, or even better than, catalysts reported in the literature, with a HGR of 4363 mL min^{-1} g_{cast}^{-1} and a low activation energy of 8.59 kJ mol^{-1} under specific conditions. Furthermore, reuse assays indicated excellent catalyst stability, with a significant reduction in activity observed only after sixteen cycles, attributed to the formation of reaction byproducts. The high catalytic activity and stability of the Pt NPs/$MnWO_4$ material position it as

a promising catalyst for hydrogen production reactions, aligning with contemporary sustainable development goals, particularly those related to the transition to a low-carbon economy.

Supplementary Information

Supplementary data (Figures S1-S6) are available free of charge at http://jbcs.sbq.org.br as PDF file.

Data Availability Statement

The authors confirm that the data supporting the findings of this study are available within the text.

Acknowledgments

The authors would like to thank the Fundação Coordenação de Aperfeiçoamento de Pessoal de Nível Superior - Brazil (CAPES), Conselho Nacional de Desenvolvimento Científico e Tecnológico (CNPq); Process: 312400/2021-7, 405828/2022-5 and 407799/2022-2, the Fundação de Amparo à Pesquisa do Estado de Minas Gerais; Process: FAPEMIG RED-00144-22, APQ-01060-17, APQ-03572-23 and FAPEMIG APQ-01275-18, the Department of Chemistry of the Universidade Federal de Viçosa, the Department of Physics of the Universidade Federal de Viçosa and the Microscopy Centre of the Universidade Federal de Minas Gerais for providing equipment and technical support for electron microscopy experiments.

Author Contributions

Jorge Luiz dos Santos was responsible for data curation, formal analysis, investigation, methodology, validation, writing original draft; Iterlandes Machado Junior for data curation, formal analysis, investigation, methodology, validation, writing original draft; Gabriel Henrique Sperandio for data curation, formal analysis, investigation, methodology; Gessica C. Dias for formal analysis, investigation, methodology; Anderson Dias for conceptualization, supervision, writing (review and editing); Geraldo M. de Lima for conceptualization, supervision, writing (review and editing); Renata P. L. Moreira for conceptualization, funding acquisition, project administration, supervision, writing (review and editing).

References

1. Lapi, T.; Chatzimpiros, P.; Raineau, L.; Prinzhofer, A.; *Int. J. Hydrogen Energy* **2022**, *47*, 21701. [Crossref]
2. Li, J.; Hong, X.; Wang, Y.; Luo, Y.; Huang, P.; Li, B.; Zhang, K.; Zou, Y.; Sun, L.; Xu, F.; Rosei, F.; Verevkin, S. P.; Pimerzin, A. A.; *Energy Storage Mater.* **2020**, *27*, 187. [Crossref]
3. Møller, K. T.; Jensen, T. R.; Akiba, E.; Li, H. wen; *Prog. Nat. Sci.: Mater. Int.* **2017**, *27*, 34. [Crossref]
4. Chen, B.; Chen, S.; Bandal, H. A.; Appiah-Ntiamoah, R.; Jadhav, A. R.; Kim, H.; *Int. J. Hydrogen Energy* **2018**, *43*, 9296. [Crossref]
5. Junior, I. M.; Sperandio, G. H.; Lopes, R. P.; *Int. J. Hydrogen Energy* **2024**, *53*, 1323. [Crossref]
6. Mohammad Pour, M. T.; Paydar, M. H.; *Int. J. Hydrogen Energy* **2022**, *47*, 36372. [Crossref]
7. Dragan, M.; *Catalysts* **2022**, *12*, 356. [Crossref]
8. Li, Q.; Kim, H.; *Fuel Process. Technol.* **2012**, *100*, 43. [Crossref]
9. Li, R.; Zhang, F.; Zhang, J.; Dong, H.; *Int. J. Hydrogen Energy* **2022**, *47*, 5260. [Crossref]
10. Jeong, S. U.; Kim, R. K.; Cho, E. A.; Kim, H. J.; Nam, S. W.; Oh, I. H.; Hong, S. A.; Kim, S. H.; *J. Power Sources* **2005**, *144*, 129. [Crossref]
11. Ye, W.; Zhang, H.; Xu, D.; Ma, L.; Yi, B.; *J. Power Sources* **2007**, *164*, 544. [Crossref]
12. Xu, D.; Dai, P.; Liu, X.; Cao, C.; Guo, Q.; *J. Power Sources* **2008**, *182*, 616. [Crossref]
13. Seven, F.; Sahiner, N.; *J. Power Sources* **2014**, *272*, 128. [Crossref]
14. Marchionni, A.; Bevilacqua, M.; Filippi, J.; Folliero, M. G.; Innocenti, M.; Lavacchi, A.; Miller, H. A.; Pagliaro, M. V.; Vizza, F.; *J. Power Sources* **2015**, *299*, 391. [Crossref]
15. Kim, K.; Kim, T.; Lee, K.; Kwon, S.; *J. Power Sources* **2011**, *196*, 9069. [Crossref]
16. Li, H.; Liao, J.; Zhang, X.; Liao, W.; Wen, L.; Yang, J.; Wang, H.; Wang, R.; *J. Power Sources* **2013**, *239*, 277. [Crossref]
17. Zhu, J.; Li, R.; Niu, W.; Wu, Y.; Gou, X.; *J. Power Sources* **2012**, *211*, 33. [Crossref]
18. Balbay, A.; Saka, C.; *Energy Sources, Part A* **2018**, *40*, 794. [Crossref]
19. Kılınç, D.; Şahin, Ö.; *Int. J. Hydrogen Energy* **2019**, *44*, 18858. [Crossref]
20. Coelho, L. O.; Sperandio, G. H.; Chagas da Silva, R.; Lopes Moreira, R. P.; de Jesus, J. R.; *Processes* **2024**, *12*, 2342. [Crossref]
21. Seven, F.; Sahiner, N.; *Int. J. Hydrogen Energy* **2014**, *39*, 15455. [Crossref]
22. Şahin, Ö.; Saka, C.; Baytar, O.; Hansu, F.; *J. Power Sources* **2013**, *240*, 729. [Crossref]
23. Patel, N.; Patton, B.; Zanchetta, C.; Fernandes, R.; Guella, G.; Kale, A.; Miotello, A.; *Int. J. Hydrogen Energy* **2008**, *33*, 287. [Crossref]
24. Uzundurukan, A.; Devrim, Y.; *Int. J. Hydrogen Energy* **2019**, *44*, 17586. [Crossref]
25. Bai, Y.; Wu, C.; Wu, F.; Yi, B.; *Mater. Lett.* **2006**, *60*, 2236. [Crossref]
26. Doherty, S.; Knight, J. G.; Alharbi, H. Y.; Paterson, R.; Wills, C.; Dixon, C.; Šiller, L.; Chamberlain, T. W.; Griffiths, A.; Collins,

S. M.; Wu, K.; Simmons, M. D.; Bourne, R. A.; Lovelock, K. R. J.; Seymour, J.; *ChemCatChem* **2022**, *14*, 1752. [Crossref]
27. Liu, Z.; Guo, B.; Chan, S. H.; Tang, E. H.; Hong, L.; *J. Power Sources* **2008**, *176*, 306. [Crossref]
28. Larichev, Y. V.; Netskina, O. V.; Komova, O. V.; Simagina, V. I.; *Int. J. Hydrogen Energy* **2010**, *35*, 6501. [Crossref]
29. Shang, Y.; Chen, R.; Jiang, G.; *Int. J. Hydrogen Energy* **2008**, *33*, 6719. [Crossref]
30. Zhou, S.; Cheng, L.; Huang, Y.; Liu, Y.; Shi, L.; Isimjan, T. T.; Yang, X.; *Appl. Catal., B* **2023**, *328*, 122519. [Crossref]
31. Chen, C. W.; Chen, C. Y.; Huang, Y. H.; *Int. J. Hydrogen Energy* **2009**, *34*, 2164. [Crossref]
32. Hsueh, C. L.; Chen, C. Y.; Ku, J. R.; Tsai, S. F.; Hsu, Y. Y.; Tsau, F.; Jeng, M. S.; *J. Power Sources* **2008**, *177*, 485. [Crossref]
33. Xia, Z. T.; Chan, S. H.; *J. Power Sources* **2005**, *152*, 46. [Crossref]
34. Amendola, S. C.; Sharp-Goldman, S. L.; Saleem Janjua, M.; Kelly, M. T.; Petillo, P. J.; Binder, M.; *J. Power Sources* **2000**, *85*, 186. [Crossref]
35. Sperandio, G.; Machado Jr., I.; Bernardo, E.; Moreira, R.; *Processes* **2023**, *11*, 3250. [Crossref]
36. dos Reis, T. M.; Alves, A. C. C.; da Silva, V. N.; Siqueira, G. O.; de Andrade, F. V.; de Lima, G. M.; Moreira, R. P. L.; *Processes* **2024**, *12*, 2340. [Crossref]
37. Sperandio, G. H.; de Carvalho, J. P.; de Jesus, C. B. R.; Machado Jr., I.; de Oliveira, K. L. A.; Puiatti, G. A.; de Jesus, J. R.; Moreira, R. P. L.; *Int. J. Hydrogen Energy* **2024**, *83*, 774. [Crossref]
38. Chen, Y.; Kim, H.; *Mater. Lett.* **2008**, *62*, 1451. [Crossref]
39. Peña-Alonso, R.; Sicurelli, A.; Callone, E.; Carturan, G.; Raj, R.; *J. Power Sources* **2007**, *165*, 315. [Crossref]
40. Krishnan, P.; Yang, T. H.; Lee, W. Y.; Kim, C. S.; *J. Power Sources* **2005**, *143*, 17. [Crossref]
41. Kumar, S.; Kumar, R.; Goyal, N.; Yadav, A.; Sahoo, B.; *ACS Appl. Nano Mater.* **2024**, *7*, 16422. [Crossref]
42. Shaban, M.; Binsabt, M.; Ahmed, A. M.; Mohamed, F.; *Nanomaterials* **2021**, *11*, 3445. [Crossref]
43. Şen, B.; Demirkan, B.; Levent, M.; Şavk, A.; Şen, F.; *Int. J. Hydrogen Energy* **2018**, *43*, 20234. [Crossref]
44. Nouruzi, N.; Dinari, M.; Gholipour, B.; Mokhtari, N.; Farajzadeh, M.; Rostamnia, S.; Shokouhimehr, M.; *Mol. Catal.* **2022**, *518*, 112058. [Crossref]
45. Liu, P.; Gu, X.; Kang, K.; Zhang, H.; Cheng, J.; Su, H.; *ACS Appl. Mater. Interfaces* **2017**, *9*, 10759. [Crossref]
46. Joaquín-Morales, M. G.; Fuentes, A. F.; Montemayor, S. M.; Meléndez-Zaragoza, M. J.; Gutiérrez, J. M. S.; Ortiz, A. L.; Collins-Martínez, V.; *Int. J. Hydrogen Energy* **2019**, *44*, 12390. [Crossref]
47. Sethi, Y. A.; Kulkarni, A. K.; Ambalkar, A. A.; Khore, S. K.; Gunjal, A. R.; Gosavi, S. W.; Kale, B. B.; *Nanoscale Adv.* **2021**, *3*, 508. [Crossref]
48. Sobhani-Nasab, A.; Pourmasoud, S.; Ahmadi, F.; Wysokowski, M.; Jesionowski, T.; Ehrlich, H.; Rahimi-Nasrabadi, M.; *Mater. Lett.* **2019**, *238*, 159. [Crossref]
49. Hoang, L. H.; Van Hanh, P.; Phu, N. D.; Chen, X. B.; Chou, W. C.; *J. Phys. Chem. Solids* **2015**, *77*, 122. [Crossref]
50. Naik, K. K.; Gangan, A. S.; Pathak, A.; Chakraborty, B.; Nayak, S. K.; Rout, C. S.; *ChemistrySelect* **2017**, *2*, 5707. [Crossref]
51. Yesuraj, J.; Elanthamilan, E.; Muthuraaman, B.; Suthanthiraraj, S. A.; Merlin, J. P.; *J. Electron. Mater.* **2019**, *48*, 7239. [Crossref]
52. Askari, M. B.; Jamali, F.; Tourchi Moghadam, M. T.; Azizi, S.; Seifi, M.; *Sustainability* **2023**, *15*, 14910. [Crossref]
53. Chen, H.; Li, X.; *Russ. J. Phys. Chem. A* **2023**, *97*, 2052. [Crossref]
54. Dong, K.; Liu, Z.; Liu, J.; Huang, S.; Li, Z.; Yuan, Q.; Ren, J.; Qu, X.; *Nanoscale* **2014**, *6*, 2211. [Crossref]
55. Singh, R.; *Int. J. Hydrogen Energy* **2022**, *47*, 26549. [Crossref]
56. Siqueira, K. P. F.; Dias, A.; *J. Nanopart. Res.* **2011**, *13*, 5927. [Crossref]
57. Pirhashemi, M.; Habibi-Yangjeh, A.; *J. Mater Sci. Technol.* **2018**, *34*, 1891. [Crossref]
58. Saranya, S.; Selvan, R. K.; Priyadharsini, N.; *Appl. Surf. Sci.* **2012**, *258*, 4881. [Crossref]
59. Muthamizh, S.; Suresh, R.; Giribabu, K.; Manigandan, R.; Praveen Kumar, S.; Munusamy, S.; Narayanan, V.; *J. Alloys Compd.* **2015**, *619*, 601. [Crossref]
60. Rathi, V.; Panneerselvam, A.; Sathiyapriya, R.; *J. Mater. Sci.:Mater. Electron.* **2020**, *31*, 14823. [Crossref]
61. Kumar, K. S.; Vaishnavi, K.; Venkataswamy, P.; Ravi, G.; Ramaswamy, K.; Vithal, M.; *J. Indian Chem. Soc.* **2021**, *98*, 100140. [Crossref]
62. Peixoto, J. C.; Nogueira, A. E.; Dias, A.; Torres, J. A.; da Cruz, J. C.; Ribeiro, C.; Siqueira, K. P. F.; *Mater Res. Bull.* **2022**, *153*, 111912. [Crossref]
63. Ptak, M.; MacZka, M.; Hermanowicz, K.; Pikul, A.; Hanuza, J.; *Spectrochim. Acta., Part A* **2012**, *86*, 85. [Crossref]
64. Zou, X. X.; Li, G. D.; Wang, P. P.; Su, J.; Zhao, J.; Zhou, L. J.; Wang, Y. N.; Chen, J. S.; *Dalton Trans.* **2012**, *41*, 9773. [Crossref]
65. Hoang, L. H.; Hien, N. T. M.; Choi, W. S.; Lee, Y. S.; Taniguchi, K.; Arima, T.; Yoon, S.; Chena, X. B.; Yang, I. S.; *J. Raman Spectrosc.* **2010**, *41*, 1005. [Crossref]
66. Shivaganga, G. S.; Parameswara, P.; Mallikarjunaswamy, C.; Kumar, K. C. S.; Soundarya, T. L.; Nagaraju, G.; Punith, S.; Ranganatha, V. L.; *J. Mater. Sci.:Mater. Electron.* **2023**, *34*, 1791. [Crossref]
67. Lei, S.; Tang, K.; Fang, Z.; Huang, Y.; Zheng, H.; *Nanotechnology* **2005**, *16*, 2407. [Crossref]
68. Assis, M.; Tello, A. C. M.; Abud, F. S. A.; Negre, P.; Ribeiro, L. K.; Ribeiro, R. A. P.; Masunaga, S. H.; Lima, A. E. B.; Luz, G. E.; Jardim, R. F.; Silva, A. B. F.; Andrés, J.; Longo, E.; *Appl. Surf. Sci.* **2022**, *600*, 154081. [Crossref]

69. Trombetta, F.; Lima, D. W.; Fiegenbaum, F.; Becker, M. R.; de Souza, M. O.; Martini, E. M. A.; *Int. J. Hydrogen Energy* **2018**, *43*, 6945. [Crossref]
70. Biehler, E.; Quach, Q.; Abdel-Fattah, T. M.; *Nanomaterials* **2023**, *13*, 1994. [Crossref]
71. Altaf, C. T.; Minkina, V. G.; Shabunya, S. I.; Colak, T. O.; Sankir, N. D.; Sankir, M.; Kalinin, V. I.; *ACS Omega* **2023**, *8*, 36100. [Crossref]
72. Kojima, Y.; Suzuki, K.-I.; Fukumoto, K.; Sasaki, M.; Yamamoto, T.; Kawai, Y.; Hayashi, H.; *Int. J. Hydrogen Energy* **2002**, *27*, 1029. [Crossref]
73. Akbayrak, S.; Özkar, S.; *J. Colloid Interface Sci.* **2021**, *596*, 100. [Crossref]
74. Bousada, G. M.; Nogueira da Silva, V.; Fernandes de Souza, B.; de Oliveira, R. S.; Machado Jr., I.; da Cunha, C. H. F.; Astruc, D.; Teixeira, R. R.; Lopes Moreira, R. P.; *RSC Adv.* **2024**, *14*, 19459. [Crossref]
75. Huff, C.; Biehler, E.; Quach, Q.; Long, J. M.; Abdel-Fattah, T. M.; *Colloids Surf., A* **2021**, *610*. [Crossref]
76. Shang, Y.; Chen, R.; *Energy Fuels* **2006**, *20*, 2142. [Crossref]
77. Patel, N.; Fernandes, R.; Miotello, A.; *J. Power Sources* **2009**, *188*, 411. [Crossref]

Submitted: May 13, 2025
Final version online: July 15, 2025